High-efficiency and ultra-thin electromagnetic wave absorption xAl2O3-(1-x)Sr0.85Gd0.15TiO3 ceramics in X-band

Hui Xie (xiehuixihang@163.com)
Xi'an Aeronautical University
Chaoqun Yang
Xi'an Technological University
Yingying Zhou
Xi'an Aeronautical University
Zhaowen Ren
Northwestern Polytechnical University
Ping Liu
Xi'an Technological University

Research Article

Keywords: SrTiO3, Ceramic, Microwave absorption, Hot-press sintering

DOI: https://doi.org/10.21203/rs.3.rs-26498/v1

Abstract

$x$$Al_2O_3$-(1-$x$)$Sr_{0.85}Gd_{0.15}TiO_3$($x$=0.2, 0.3, 0.4, 0.5) ceramics were fabricated by hot-press sintering. Their morphology, phase composition, conductivity, dielectric properties as well as microwave absorption performance were examined by scanning electron microscopy (SEM), X-ray diffraction (XRD), multifunction digital four-probe meter and vector network analysis, respectively. The microwave absorption of as-prepared $x$$Al_2O_3$-(1-$x$)$Sr_{0.85}Gd_{0.15}TiO_3$ ceramics demonstrates excellent microwave absorbability. It is unexpectedly found that with a thickness of only 0.346 mm, $x$$Al_2O_3$-(1-$x$)$Sr_{0.85}Gd_{0.15}TiO_3$ (x=0.2) ceramic exhibits an absorption bandwidth of 3.7 GHz (8.7-12.4 GHz), being consequential to reflection loss less than -10 dB (over 90% of microwave absorption). It is as well discovered that the minimum reflection loss and absorption peak frequency of $x$$Al_2O_3$-(1-$x$)$Sr_{0.85}Gd_{0.15}TiO_3$ (x=0.3) with a thickness of 0.436 mm were -45.43 dB and 11.3 GHz, respectively. The prominent microwave absorption performance of the ceramic with such a thin thickness can be attributed to strong interfacial polarization, dielectric frequency dispersion, and good electromagnetic impedance matching. It indicates that the $x$$Al_2O_3$-(1-$x$)$Sr_{0.85}Gd_{0.15}TiO_3$ ceramics with appropriate Al_2O_3 mass fraction and thickness showing good potential for effective microwave absorbing materials.

Introduction

With the speedy evolution of science and technology in the defense industry, the demands of electromagnetic microwave absorbing materials that can effectively reduce the reflection of electromagnetic waves at high temperature in a required frequency range are urgent [1-4]. Therefore, the tremendous emphasis has been made to high-temperature microwave absorption materials due to their better microwave attenuation capability, and many of them have been synthesized and used to suppress radar detection in militarily [5-8]. In recent years, perovskite structured materials (e.g. $SrTiO_3$, $BaTiO_3$ and $CaTiO_3$) have been extensively researched owning to their potential applications, such as capacitor, photo-corrosion, solar cell, sensor, superconductor and so on [9-11]. In particular, $SrTiO_3$, as a member of perovskite structure materials family, has attracted increasing interest in dielectric properties and microwave absorption properties owing to its adjustable dielectric loss, low cost, and excellent temperature stability [12-14]. The most concerning advantage of such $SrTiO_3$ perovskite material is the flexible chemical composition by A- or B-site doping, by which one can adjust the electronic states. Therefore, the dielectric properties of $SrTiO_3$ ceramic depend not only on the synthesis process and particle size, but also on the doping element kind and amount [15]. In order to enhance the microwave absorbing property of $SrTiO_3$, various transition metals and rare earth ions were used as dopants [16, 17]. For example, when $SrTiO_3$ was doped with rare earth elements, a vast number of defects and oxygen vacancies came forth [18]. The suitable substitution (La^{3+}/Gd^{3+} in Sr^{2+} site) can effectively change the carrier concentration of $SrTiO_3$ and microwave dielectric properties [18-20].

Al_2O_3, as a metal oxide material, is widely used as a ceramic matrix to change physical properties of additive, due to its excellent properties such as low density, high strength, high hardness, oxidation resistance, corrosion resistance and excellent electrical insulation, etc., in national defense, aviation, aerospace and other fields [21]. Therefore, Al_2O_3 is usually used as impedance matching regulator combined with ceramic absorbent to form ceramic composite absorbing material. In recently, some researchers have demonstrated the electromagnetic and microwave absorption properties of $SrTiO_3/Al_2O_3$ complex ceramics [22, 23]. However, the microwave absorbing property of rare earth element doped-$SrTiO_3/Al_2O_3$ has not been reported previously.

In this study, Gd doped $SrTiO_3$ with different contents of Al_2O_3 were combined as ceramic composite absorbing material using hot-pressed sintering method. The microwave absorbing property in the X band was studied initially. Additionally, the influence of Al_2O_3 content on the microstructure, dielectric behavior, electrical properties, and microwave absorption performances was studied.

Experimental

2.1 Fabrication of $x Al_2O_3$-(1-x)$Sr_{0.85}Gd_{0.15}TiO_3$

$x Al_2O_3$-(1-x)$Sr_{0.85}Gd_{0.15}TiO_3$ ceramics with different x values (x=0.2, 0.3, 0.4, and 0.5) were prepared by hot-press sintering. All raw materials including TiO_2 (CP), $SrCO_3$ (AR), Gd_2O_3 (99.999%) and Al_2O_3 (AR) were acquired from Sinopharm Chemical Reagent Co., Ltd. Firstly, TiO_2, $SrCO_3$, and Gd_2O_3 were mixed in ethanol and ball-milled according to the stoichiometric ratio of $Sr_{0.85}Gd_{0.15}TiO_3$, where the ball milling speed is 300 rpm. After 12 h of ball milling, the mixture was dried in an oven at 80℃ for 5 h and sifted with a 100-mesh sieve. Secondly, the mixture was pre-calcined for 3 h at 1300℃ in an alumina crucible to obtain $Sr_{0.85}Gd_{0.15}TiO_3$ powder. Subsequently, $Sr_{0.85}Gd_{0.15}TiO_3$ and Al_2O_3 powder were mixed in proportion by ball milling at 300 rpm for 12 h and dried at 80℃ for 5 h. In order to obtain high density ceramics, they were prepared by hot-press sintering at 1350℃ under 30 MPa for 2 h with a graphite mold in vacuum. Eventually, the as-prepared complex ceramics were cooled down followed by furnace cooling to room temperature in the vacuum hot pressing sintering furnace.

2.2 Characterization

Phase compositions and crystalline structure of these samples were observed using X-ray powder diffraction (XRD, X'Pert PRO, PANalytical) with CuK radiation at room temperature. The XRD patterns were measured from 10° to 90° at 4°/min. Field-emission scanning electron microscopy (SEM, VEGA3 SBH, TESCAN, Czech Republic) was used to characterize the microstructure features and morphology of the fracture cross-section of the sintered ceramics. The direct current (DC) electrical conductivities were examined by the ST2235 multifunction digital four-probe tester. The apparent density and relative density were tested using the Archimedean method based on the ASTMC 373-88 standard. The prepared ceramics were split up rectangular bars with 22.86×10.16×2.00 mm and a vector network analyzer

(E8362B, Agilent technology, USA) was utilized to measure the complex permittivity by the waveguide method in X-band (8.2~12.4 GHz).

Result And Discussion

3.1 Phase composition analysis

XRD patterns of $x$$Al_2O_3$-(1-$x$)$Sr_{0.85}Gd_{0.15}TiO_3$ ceramics with different x values are displayed in Fig. 1. For each sample, the primary phase is the perovskite phase of $SrTiO_3$ (PDF#: 89-4934) and mixed with diffraction peaks of Al_2O_3 and the impurity phase of $SrAl_{12}O_{19}$ (PDF#: 70-0947), which may be related to the chemical reaction. It can be inferred that during sintering process, $SrTiO_3$ reacted with partial Al_2O_3 to form $SrAl_{12}O_{19}$ in all samples by solid-state diffusion at high temperature in the reduction atmosphere. Therefore, each sample exhibits multiple phases of $SrTiO_3$, $SrAl_{12}O_{19}$ and Al_2O_3. Furthermore, XRD analysis indicates that the diffraction peak intensities of Al_2O_3 and $SrAl_{12}O_{19}$ rise gradually with the increasing adding content of Al_2O_3 from 20 wt.% to 50 wt.%. It can also be seen that all the samples show similar patterns indicating that the $Sr_{0.85}Gd_{0.15}TiO_3$ are crystallized into a cubic perovskite structure.

There is another issue worthy noting that the standard lattice parameter of $SrTiO_3$ is 3.905 Å (ICSD-94573) [24], which is larger than $x$$Al_2O_3$-(1-$x$)$Sr_{0.85}Gd_{0.15}TiO_3$ with different x values (x=0.2, 3.89695 Å, x=0.3, 3.89104 Å, x=0.4, 3.89064 Å and x=0.5, 3.88755 Å). This may be attributed to two aspects: on the one hand, the Sr^{2+} (ion radius 1.44 Å) [25] are replaced by the smaller Gd^{3+} (ion radius 1.195 Å) [21]; On the other hand, the B-site Ti^{4+} (0.605 Å) [26] are partly substituted by Al^{3+} (0.57 Å) [27].

3.2 Morphology analysis

Fig. 2 displays both SE and BSE images of the fractured cross-sections of $x$$Al_2O_3$-(1-$x$)$Sr_{0.85}Gd_{0.15}TiO_3$ ceramics. These photos are from the fracture surface of the ceramic samples. Different microstructures, especially grain size, can be observed obviously, which changes over the adding Al_2O_3 contents. It also indicates that all the $x$$Al_2O_3$-(1-$x$)$Sr_{0.85}Gd_{0.15}TiO_3$ ceramics have high density in microstructures, indicating the ceramics are dense, well-sintered, and nearly non-porous. The relative densities of all ceramics are more than 97.5 % (Table 1).

It can be indicated from the BSE photos in Fig. 2(b, d, f, h), the bright region become smaller with the increasing adding Al_2O_3 content, however, dark region gradually grows.

Combing with the XRD observations in Fig. 1, it can be derived that the bright region stands for $Sr_{0.85}Gd_{0.15}TiO_3$ and the dark region symbolizes Al_2O_3 and $SrAl_{12}O_{19}$. Meanwhile, the secondary phase $SrAl_{12}O_{19}$ gradually becomes uniform with the increasing of the adding Al_2O_3 content. This result is in line with the XRD result as shown in Fig. 1. There is a factor that can be used to explain this phenomenon: The atomic number and backscattered electron yield have an important effect on the variation of the BSE signal [23]. Therefore, the distribution of constituent chemical elements of a sample can be visualized by BSE images, and the greater the atomic number of the chemical element is, the brighter the contrast there is displayed in BSE images.

Table 1 The apparent and relative densities of the as-prepared ceramics.

Sample	Apparent density (g/cm^3)	Relative density (%)
20%A+SGT	4.753	98.3
30%A+SGT	4.592	97.7
40%A+SGT	4.437	97.9
50%A+SGT	4.302	98.1

3.3 Electrical conductivity

The dependence of electrical conductivity on Al_2O_3 contents of $x$$Al_2O_3$-(1-$x$)$Sr_{0.85}Gd_{0.15}TiO_3$ ceramics is presented in Fig. 3. In this study, the conductivity determined by the 4-probe DC measurement is the total conductivity. In general, $SrTiO_3$ is one kind of insulators and it possesses weak electrical conductivity [16]. However, the electrical conductivity can be improved by doping high valence ions. From Fig. 3, it could be contended that the electrical conductivity of the ceramic gradually decreases as the Al_2O_3 content increases. It can be explained by two factors: on the one instance, the content of the Al_2O_3 is gradually increased while the $Sr_{0.85}Gd_{0.15}TiO_3$ content decreased, which leads to the conductivity of the sample declined. The above phenomenon is mainly due to the conductivity of Al_2O_3 is lower than $Sr_{0.85}Gd_{0.15}TiO_3$; on the second instance, the ionic conductivity is a result of the oxygen vacancies that form for electroneutrality [23]. Due to the decrease of $Sr_{0.85}Gd_{0.15}TiO_3$, the concentration of the Gd^{3+} replaced Sr^{2+} in the A-site was decreased. According to charge compensation mechanisms, the content of oxygen vacancy is reduced as the decrease of Gd^{3+} content. At the same time, the concentration of

carriers declined, which results in the conductivity of the entire ceramics decreased. As a conclusion, conductivity decreased notably with an increase in the concentration of Al_2O_3.

3.4 Dielectric properties

It is well identified that the microwave absorbing performances of materials are mainly administered by the relative complex permittivity (and permeability ([28, 29]. The frequency dependence of and for the ceramics was measured by a vector network analyzer, as presented in Fig. 4. It is unambiguous that the complex permittivity of $x$$Al_2O_3$-(1-$x$)$Sr_{0.85}Gd_{0.15}TiO_3$ is a functional of frequency in the measured frequency range of X-band for the ceramics. The real part of complex permittivity ( ) represents the electric energy storage capability, and the imaginary part of complex permittivity ( ) symbolize the electric energy loss capability, respectively [30]. It is considered that the variation of Al_2O_3 adding content results in the change of and . As shown in Fig. 4 (a), decreases as the raising of x value in $x$$Al_2O_3$-(1-$x$)$Sr_{0.85}Gd_{0.15}TiO_3$ ceramics. For instance, dramatically decreases from 678.58 to 329.16 at 8.2 GHz when the Al_2O_3 content changes from 20 wt.% to 50 wt.%. This can be explained as follows. Introducing Gd in $SrTiO_3$ could provoke lattice distortion and break the polarity of the cubic $SrTiO_3$, therefore inducing defect dipoles. Therefore, induced defect dipoles would reorient towards the electromagnetic field direction when $Sr_{0.85}Gd_{0.15}TiO_3$ was exposed to the electromagnetic field, leading to orientational polarization. With x value increases, the content of $Sr_{0.85}Gd_{0.15}TiO_3$ decreases, resulting in the reduced orientational polarization. In addition, it can be noted that the of the ceramics decreases gradually as frequency increases, presenting distinct frequency dispersion behaviors and induced by the polarization, which is advantageous to broadening the microwave absorption bandwidth. Fig. 4 (b) exhibits the of the ceramics with different Al_2O_3 contents, which confirms the existence of multiple relaxation processes in all samples. As display in Fig. 4 (b), increases gradually with the value of x rising in $x$$Al_2O_3$-(1-$x$)$Sr_{0.85}Gd_{0.15}TiO_3$ samples except for sample x=0.2. The higher indicates a better dielectric loss capacity in the electromagnetic wave range. Moreover, these samples possess multiple loss peaks with all Al_2O_3 contents. This may be contributed to multiple polarization and relaxation processes, accompanying with interfacial polarization, orientational polarization, and defect dipole polarization [23]. Figure 4 (c) displays dielectric loss tangent (tan) that is universally implemented to assess the dielectric loss capacity of microwave absorbing materials. It is unequivocal that the dielectric loss enhances prominently overall with increasing Al_2O_3 content in the ceramics.

3.5 Microwave absorption properties

Generally, excellent impedance matching between the surface of absorbing materials and atmosphere can prevent the electromagnetic wave from reflecting before it spreading into absorbing materials. Additionally, electromagnetic wave can be strongly absorbed through the high capability of dissipation and attenuation of absorbing materials. These two factors (i.e. impedance matching and high attenuation capability) are fundamental to an outstanding microwave absorbing material [31]. The reflection loss (RL) value of the complex ceramics was simulated by calculating the complex permittivity and thickness based on the transmission line theory, displayed as follows. [32, 33]:

[Please see the supplementary files section to view the equations.] (1)

(2)

Herein, Z_{in} is the normalized input impedance at the junction between atmosphere and ceramics, is the normalized impedance of free space that is 1. =1 for nonmagnetic material in any circumstance, is the frequency of electromagnetic wave, is the thickness of the ceramics and is the velocity of light. According to Eq (1) and (2), it is not difficult to draw that both the frequency range of absorption peak and thickness of the microwave absorbing materials are important to fix the practical application fields of it.

Fig. 5 (a)-(d) exhibit the frequency-dependent calculated RL values of $x$$Al_2O_3$-(1-$x$)$Sr_{0.85}Gd_{0.15}TiO_3$ ceramics with different Al_2O_3 adding contents and thicknesses. As can be seen from Fig 5(a), when the adding amount of Al_2O_3 is 20 wt.%, the minimum RL (RL_{min}) value is -40.43 dB at 9.06 GHz with a thickness of only 0.346 mm. Besides, the absorbing bandwidth when RL≤−10 dB (RL_{-10}) is 3.7 GHz covered from 8.7 to 12.4 GHz. For 30% A+SGT, it is observed that the RL_{min} value can reach to -45.43 dB at 11.26 GHz with a thickness of only 0.436 mm and the absorption bandwidth (RL_{-10}) is 3.2 GHz (9.2-12.4 GHz). The absorption bandwidth (RL_{-10}) of 40% A+SGT and 50% A+SGT is 3.3 GHz (8.9-12.2 GHz) and 1.9 GHz (10.5-12.4 GHz), respectively.

Table 2 Microwave absorbing properties of $x$$Al_2O_3$-(1-$x$)$Sr_{0.85}Gd_{0.15}TiO_3$ and other microwave absorption materials.

Absorbent and content	Thickness (mm)	Bandwidth (RL<-10 dB) (GHz)	RL_{min} (dB)	Refs.
80 wt.% $Sr_{0.85}Gd_{0.15}TiO_3$	0.346	3.7	-40.43	This work
70 wt.% $Sr_{0.85}Gd_{0.15}TiO_3$	0.436	3.2	-45.43	This work
60 wt.% $Sr_{0.85}Gd_{0.15}TiO_3$	0.468	3.3	-41.34	This work
50 wt.% $Sr_{0.85}Gd_{0.15}TiO_3$	0.479	1.9	-42.95	This work
$0.95SrTiO_{3-\delta}+0.05SrAl_{12}O_{19}$	0.234	1.4	-13.8	23
70wt.%$BaFe_{12}O_{19}$+30wt.%$Ni_{0.5}Zn_{0.5}Fe_2O_4$	2.2	1.2	-38	34
50 wt.% 6H-SiC+0.2 wt.%MWCNT	2.3	1.6	-58.9	35
70wt.% polypyrrole/Fe_3O_4	2.5	4	-41.6	36
60 wt.% C@$NiCo_2O_4$@Fe_3O_4	3.4	2.1	-43	37
50 wt.% MXene($Ti_3C_2T_x$)/Co_3O_4	2	6.2	-35	38
30 vol% $BaFe_{12}O_{19}$@C	2.11	6.6	-56.95	39
40 wt.% C@Fe_2O_3@MWCNTs	1.5	4.6	-20.6	40
30 wt.%	2	3.25	-42.53	41

Ti@MWCNTs/Fe				
30 vol% RGO/CeO_2	2	4.3	-24.4	42
28vol%$Ce_2Fe_{17}N_{3-\delta}$+Co-based microwires gridding	1.36	3.6	-20.86	43
40 wt.% Nd_2Fe_{17}	1.8	3.8	-32.5	44
30 wt.% short carbon fibers@TiO_2	1	2.4	-14.9	45

The microwave absorption properties of $x$$Al_2O_3$-(1-$x$)$Sr_{0.85}Gd_{0.15}TiO_3$ ceramic materials prepared in this work and other typical microwave absorption materials are listed in Table 2. Absorbing materials with wider absorption bandwidth lower than −10 dB are highly demanded in the EWM application. To this end, the bandwidth of RL_{-10} was highlighted for comparison in Table 2. From Table 2, it can be discovered that compared with other microwave absorption materials, the $x$$Al_2O_3$-(1-$x$)$Sr_{0.85}Gd_{0.15}TiO_3$ ceramic composites possess wider effective absorption bandwidth, stronger absorbing peaks, and obviously thinner. Consequently, $x$$Al_2O_3$-(1-$x$)$Sr_{0.85}Gd_{0.15}TiO_3$ ceramic materials with ultra-thin and excellent microwave absorption properties provide an attractive option for electromagnetic wave absorption applications.

Furthermore, Fig. 5 shows that the frequency of absorption peak shift to the left as the thickness increases, resulting in the RL peaks shift to lower frequency range. For the ceramics explored in this work, the quarter-wavelength matching model can be implemented to interpret this phenomenon. In addition, the correlation between the thickness and RL peaks obey the formula as following [46-48]:

[Please see the supplementary files section to view the equations.]

(3)

Herein, and are the matching frequency of absorption peak and the matching thickness of absorber, is the imaginary parts of complex permeability that value is 1. Accordingly, as the matching thickness increases, the RL peak shifts to the lower frequency.

Especially, there are many advantages for the $x$$Al_2O_3$-(1-$x$)$Sr_{0.85}Gd_{0.15}TiO_3$ ceramics as microwave absorbing materials, such as wide absorbing bandwidth, ultra-thin thickness and strong absorption. As described above, these advantages are mainly attributed to the high real part of permittivity, the relatively favorable imaginary part of permittivity, enhanced impedance matching characteristic and attenuation matching characteristic. As we all know, the effective microwave absorption performance should satisfy not only microwave attenuation but also impedance matching [49, 50]. To achieve the perfect impedance matching, the impedance value of free space and absorbing material should be as equal as possible. Nevertheless, for the microwave attenuation, it is necessary to make as much as possible microwave dissipation and attenuation within the interior of the microwave absorbing materials. The strong dielectric dispersion of $x$$Al_2O_3$-(1-$x$)$Sr_{0.85}Gd_{0.15}TiO_3$ is beneficial to balance these two contradictory requirements for making it as exceptional microwave absorption material. Meanwhile, the multiple interfaces among $Sr_{0.85}Gd_{0.15}TiO_3$, Al_2O_3, and $SrAl_{12}O_{19}$ can be considered as capacitor-like structures, which demonstrates a significant contribution to electromagnetic wave attenuation. Consequently, the prepared $x$$Al_2O_3$-(1-$x$)$Sr_{0.85}Gd_{0.15}TiO_3$ ceramics have a great potential for producing microwave absorbing materials with ultra-thin thickness and high-performance properties.

Conclusions

In summary, $x$$Al_2O_3$-(1-$x$)$Sr_{0.85}Gd_{0.15}TiO_3$ ceramics were prepared by hot-press sintering. The influence of Al_2O_3 content on the electrical conductivity, dielectric, and microwave absorption performance of the complex ceramics were also explored. When the Al_2O_3 content is 20 wt.%, the ceramic shows exceptional microwave absorbing performance that the minimum reflection loss reaches -40.43 dB at 9.06 GHz with a thickness of only 0.346 mm and the absorption bandwidth less than -10 dB is 3.7 GHz (8.7-12.4 GHz). The microwave absorption properties of $x$$Al_2O_3$-(1-$x$)$Sr_{0.85}Gd_{0.15}TiO_3$ ceramics with other Al_2O_3 contents prepared in this work are also excellent. It indicates that the $x$$Al_2O_3$-(1-$x$)$Sr_{0.85}Gd_{0.15}TiO_3$ ceramics with fitting constituent and thickness have the great potential and promising applications in the microwave absorption field. It was also found that the microwave dielectric properties were heavily influenced by the Al_2O_3 content, indicating that we can obtain the ideal material with excellent microwave absorption performance by controlling the amount of Al_2O_3.

Acknowledgements

This work was financially supported by the National Nature Science Foundation of China (Grant No. 51701148), Natural Science Basic Research Plan in Shaanxi Province of China (Grant No. 2019JQ-916) and Key Laboratory of Photoelectric Functional Materials and Devices, Shaanxi (Grant No. 2015szsj-59-1).

References

[1] L. Wang, H.D. Xiong, S.U. Rehman, Q.L. Tan, Y. Chen, L.L. Zhang, J.P. Yang, F.Z. Wu, M.L. Zhong, Z.C. Zhong, Microwave absorbing property enhancement of FeSiCr nanomaterials by regulating nanoparticle size, J. Alloy. Compd. 803 (2019) 631-636.

[2] Y.C. Qing, L.Y. Ma, X.C. Hu, F. Luo, W.C Zhou, $NiFe_2O_4$ nanoparticles filled $BaTiO_3$ ceramics for high-performance electromagnetic interference shielding applications, Ceram. Int. 44 (2018) 8706-8709.

[3] F. Wan□J.H. Yan□H.M. Xu, Enhanced microwave absorbance of oxidized $SiC_f/AlPO_4$, composites via the formation of a carbon layer on the SiC fibre surface, J. Eur. Ceram. Soc. 38 (2018) 4356-4362.

[4] L.B. Kong, Z.W. Li, L. Liu, R. Huang, M. Abshinova, Z.H. Yang, C.B. Tang, P.K. Tan, C. R. Deng, S. Matitsine, Recent progress in some composite materials and structures for specific electromagnetic applications, Int. Mater. Rev. 58 (2013) 203-259.

[5] Y.C. Qing, Q.L. Wen, F. Luo, W.C. Zhou, Temperature dependence of the electromagnetic properties of graphene nanosheet reinforced alumina ceramics in the X-band, J. Mater. Chem. 4 (2016) 4853-4862.

[6] Y.K. Dou, J.B. Li, X.Y. Fang, H.B. Jin, M.S. Cao, The enhanced polarization relaxation and excellent high-temperature dielectric properties of N-doped SiC, Appl. Phys. Lett. 104 (2014) 052102.

[7] X.Y. Yuan, L.F. Cheng, Y.J. Zhang, S.W. Guo, L.T. Zhang, Fe-doped SiC/SiO_2 composites with ordered inter-filled structure for effective high-temperature microwave attenuation, Mater. Design. 92 (2016) 563-570.

[8] J. Yuan, H.J. Yang, Z.L. Hou, W.L. Song, H. Xu, Y.Q. Kang, H.B. Jin, X. Y. Fang, M.S. Cao, Ni-decorated SiC powders: Enhanced high-temperature dielectric properties and microwave absorption performance, Powder Technol. 237 (2013) 309-313.

[9] E. Padmini, K. Ramachandran, M. Muralidharan, Structural, optical, magnetic and dielectric properties of Dy-doped $SrTiO_3$ nano ceramics, J. Mater. Sci-Mater. El. 29 (2018) 17078-17088.

[10] E. Grabowska, Selected perovskite oxides: Characterization, preparation and photocatalytic properties—A review, Appl. Catal. B-Environ. 186 (2016) 97-126.

[11] Q. Zhang, Y. Huang, S.Q. Peng, T.T. Huang, J.J. Cao, W.K. Ho, S.C. Lee, Synthesis of $SrFe_xTi_{1-x}O_{3-\delta}$ nanocubes with tunable oxygen vacancies for selective and efficient photocatalytic NO oxidation, Appl. Catal. B-Environ. 239 (2018) 1-9.

[12] H.D. Choi, HW.W. Shim, K.Y. Cho, H.J. Lee, C.S. Park, H.G. Yoon, Electromagnetic and electromagnetic wave-absorbing properties of the $SrTiO_3$-epoxy composite, J. Appl. Polym. Sci. 72 (1999) 75- 83.

[13] D. Thomas, C. Janardhanan, M.T. Sebastian, Mechanically flexible butyl rubber-$SrTiO_3$ composite dielectrics for microwave applications, Int. J. Appl. Ceram. Technol. 8 (2011) 1099-1107.

[14] V.S. Nisa, S. Rajesh, K.P. Murali, V. Priyadarsini, S.N. Potty, R. Ratheesh, Preparation, characterization and dielectric properties of temperature stable $SrTiO_3$/PEEK composites for microwave substrate applications, Compos. Sci. Technol. 68 (2008) 106-112.

[15] T. Luo, X.X. Shan, J.W. Zhao, H.H. Feng, Q. Zhang, H.T. Yu, J.S. Liu, Improvement of quality factor of $SrTiO_3$ dielectric ceramics with high dielectric constant using Sm_2O_3, J. Am. Ceram. Soc. 102 (2019) 3849-3853.

[16] E. Bellingeri, D. Marré, I. Pallecchi, L. Pellegrino, G. Canu, A. S. Siri, Deposition of ZnO thin films on $SrTiO_3$ single-crystal substrates and field effect experiments, Thin Solid Films, 486 (2005) 186-190.

[17] K. Chandra Babu Naidu, T. Sofi Sarmash, V. Narasimha Reddy, M. Maddaiah, P. Sreenivasula Reddy, T. Subbarao, Structural, dielectric and electrical properties of La_2O_3 doped $SrTiO_3$ ceramics, J. Aust. Ceram. Soc. 51 (2015) 94-102.

[18] Y.Y. Zhou, Q.L. Wen, Z.W. Ren, H. Xie, S.P. Tao, W.C. Zhou, Gadolinium-doped strontium titanate for high-efficiency electromagnetic interference shielding, J. Alloy. Compd. 733 (2018) 33-39.

[19] M.J. Sayagués, F.J. Cotor, M. Pueyo, R. Poyato, F.J. Garcia-Garcia, Mechanosynthesis of $Sr_{1-x}La_xTiO_3$ anodes for SOFCs: Structure and electrical conductivity, J. Alloy. Compd. 763 (2018) 679-686.

[20] S.L. Chen, L.X. Li, S.H. Yu, H.R. Zheng, Z. Sun, W.J. Luo, The effects of inequivalent La^{3+} introduction on the structure and dielectric properties of $SrTiO_3$ ceramic at microwave range, Mater. Chem. Phys. 216 (2018) 339-344.

[21] Z.N. Yang, F. Luo, W.C. Zhou, D.M. Zhu, Z.B. Huang, Design of a broadband electromagnetic absorbers based on TiO_2/Al_2O_3 ceramic coatings with metamaterial surfaces, J. Alloy. Compd. 687 (2016) 384-388.

[22] S.K. Sahoo, D.C. Agrawal, D.C. Dube, Microwave dielectric ceramics in the system Al_2O_3 $SrTiO_3$, Ferroelectrics, 327 (2005) 51-56.

[23] Q.L. Wen, W.C. Zhou, H. Gao, Y.Y. Zhou, F. Luo, D.M. Zhu, Z.B. Huang, Y.C. Qing, High dielectric and microwave absorption properties of ultra-thin $(1-x)SrTiO_{3-\delta}–xSrAl_{12}O_{19}$ films, Ceram. Int. 44 (2018) 12210-12215.

[24] Z.Y. Shen, Q.G. Hu, Y.M. Li, Z.M. Wang, W.Q. Luo, Y. Hong, Z.X. Xie, R.H. Liao, Structure and dielectric properties of $Re_{0.02}Sr_{0.97}TiO_3$ (Re=La, Sm, Gd, Er) ceramics for high-voltage capacitor applications, J. Am. Ceram. Soc. 96 (2013) 2551-2555.

[25] A. Tkach, T.M. Correia, A. Almeida, J. Agostinho Moreira, M.R. Chaves, O. Okhay, P.M. Vilarinho, I. Gregora, J. Petzelt, Role of trivalent Sr substituents and Sr vacancies in tetragonal and polar states of $SrTiO_3$, Acta Mater. 59 (2011) 5388-5397.

[26] W.Q. Luo, L. Zhang, Z.Y. Shen, Structure and energy storage characteristics of charge self-compensated rare earth doped strontium titanate ceramics, China Ceram. 53 (2017) 31-35.

[27] C.W. Zhong, B. Tang, Y.D. Tan, S.R. Zhang, Impacts of Al_2O_3 doping on microstructure, phase constitution and microwave dielectric properties of $Ca_{0.61}Nd_{0.26}TiO_3$ ceramics, T. Indian Ceram. Soc. 76 (2017) 97-101.

[28] Q.Z. Jiao, Y.F. Wang, L. Hao, H.S. Li, Y. Zhao, Synthesis of magnetic nickel ferrite microspheres and their microwave absorbing properties, Chem. Res. Chin. Univ. 32 (2016) 678-681.

[29] H.J. Wei, X.W. Yin, Z.X. Hou, F.R. Jiang, H.L. Xu, M.H. Li, L.T. Zhang, L.F. Cheng, A novel SiC-based microwave absorption ceramic with $Sc_2Si_2O_7$ as transparent matrix, J. Eur. Ceram. Soc. 38 (2018) 4189-4197.

[30] X.Y. Yuan, L.F. Cheng, L.T Zhang, Electromagnetic wave absorbing properties of SiC/SiO_2 composites with ordered inter-filled structure, J. Alloy. Compd. 680 (2016) 604-611.

[31] R.W. Shu, G.Y. Zhang, X. Wang, X. Gao, M. Wang, Y. Gan, J.J. Shi, J. He, Fabrication of 3D net-like MWCNTs/$ZnFe_2O_4$ hybrid composites as high-performance electromagnetic wave absorbers, Chem. Eng. J. 337 (2018) 242-255.

[32] X.G. Huang, M.J. Zhang, Y.S. Qin, Y.Y. Chen, Bead-like Co-doped ZnO with improved microwave absorption properties, Ceram. Int. 45 (2019) 7789-7796.

[33] Y.C. Qing, W.C. Zhou, S. Jia, F. Luo, D.M. Zhu, Microwave electromagnetic property of SiO_2-coated carbonyl iron particles with higher oxidation resistance, Physica B, 406 (2011) 777-780.

[34] C. Pahwa, S.B. Narang, P. Sharma, Interfacial exchange coupling driven magnetic and microwave properties of $BaFe_{12}O_{19}/Ni_{0.5}Zn_{0.5}Fe_2O_4$ nanocomposites, J. Magn. Magn. Mater. 484 (2019) 61-66.

[35] J.S. Li, S.C. Wang, C.C. Hwang, Preparation and high-temperature microwave absorbing properties of 6H-SiC/MWCNT/silicon resin composites, Mater. Express, 10 (2020) 1-9.

[36] Y.Q. Zhan, R. Zhao, X. Xiang, S.J. He, S.M. Zhao, W.D. Xue, Hierarchical core/shell bamboo-like polypyrrole nanofibers/Fe_3O_4 hybrids with superior microwave absorption performance, Compos. Interface. 26 (2019) 1087-1100.

[37] S. Wei, X.X. Wang, B.Q. Zhang, M.X. Yu, Y.W. Zheng, Y. Wang, J.Q. Liu, Preparation of hierarchical core-shell C@$NiCo_2O_4$@Fe_3O_4 composites for enhanced microwave absorption performance, Chem. Eng.

J. 314 (2017) 477-487.

[38] R.X. Deng, B.B. Chen, H.G. Li, K. Zhang, T. Zhang, Y. Yu, L.X. Song, MXene/Co_3O_4 composite material: Stable synthesis and its enhanced broadband microwave absorption, Appl. Surf. Sci. 488 (2019) 921-930.

[39] Y.R. Liu, Y. Lin, H.B. Yang, Facile fabrication for core-shell $BaFe_{12}O_{19}$@C composites with excellent microwave absorption properties, J. Alloy. Compd. 805 (2019) 130-137.

[40] L. Wang, X.F. Yu, X. Li, J. Zhang, M. Wang, R.C. Che, Conductive-network enhanced microwave absorption performance from carbon coated defect-rich Fe_2O_3 anchored on multi-wall carbon nanotubes, Carbon, 155 (2019) 298-308.

[41] P. Bhattacharya, S. Sahoo, C.K. Das, Microwave absorption behaviour of MWCNT based nanocomposites in X-band region, Express Polym. Lett. 7 (2013) 212-223.

[42] Q. Yin, H.L. Xing, R.W. Shu, X.L. Ji, D.X. Tan, Y. Gan, Enhanced microwave absorption properties of CeO_2 nanoparticles supported on reduced graphene oxide, NANO: Brief Rep. and Rev. 11 (2016) 1650058.

[43] R.C. Hu, G.G. Tan, X.S. Gu, S.W. Chen, C.G. Wu, Q.K. Man, C.T. Chang, X.M. Wang, R.W. Li, S.L. Che, L.Q. Jiang, Electromagnetic and microwave-absorbing properties of Co-based amorphous wire and $Ce_2Fe_{17}N_{3-\delta}$ composite, J. Alloy. Compd. 730 (2018) 255-260.

[44] Z.Q. Qiao, S.K. Pan, J.L. Xiong, L.C. Cheng, P.H. Lin, J.L. Luo, Electromagnetic and microwave-absorbing properties of plate-like Nd-Ce-Fe powder, J. Electron. Mater. 46 (2017) 660-667.

[45] H.J. Wu, S.H. Qu, K.J. Lin, Y.C. Qing, L.D. Wang, Y.C. Fan, Q.H. Fu, F.L. Zhang, Enhanced low-frequency microwave absorbing property of SCFs@TiO_2 composite, Powder Technol. 333 (2018) 153-159.

[46] W.D. Zhang, Y. Zheng, X. Zhang,Q. Zhu, H.X. Yan, L.F. Liotta, H.J. Wu, S.H. Qi, Synthesis and mechanism investigation of wide-bandwidth Ni@MnO_2 NS foam microwave absorbent, J. Alloy. Compd. 792 (2019) 945-952.

[47] Z. Ma, C.T. Cao, Q.F. Liu, J.B. Wang, A new method to calculate the degree of electromagnetic impedance matching in one-layer microwave absorbers, Chinese Phys. Lett. 29 (2012) 038401.

[48] R. Joshi, C. Singh, J. Singh, D. Kaur, S. Bindra Narang, R.B. Jotania, A study of microwave absorbing properties in Co-Gd doped M-type Ba-Sr hexaferrites prepared using ceramic method, J. Mater. Sci-Mater. El. 28 (2017) 11969-11978.

[49] D. Mandal, A. Gorai, K. Mandal, Electromagnetic wave trapping in $NiFe_2O_4$ nano-hollow spheres: An efficient microwave absorber, J. Magn. Magn. Mater. 485 (2019) 43-48.

[50] L. Zhou, J.L. Huang, X.G. Wang, G.X. Su, J.Y. Qiu, Y.L. Dong, Mechanical, dielectric and microwave absorption properties of FeSiAl/Al_2O_3 composites fabricated by hot-pressed sintering, J. Alloy. Compd. 774 (2019) 813-819.

Figures

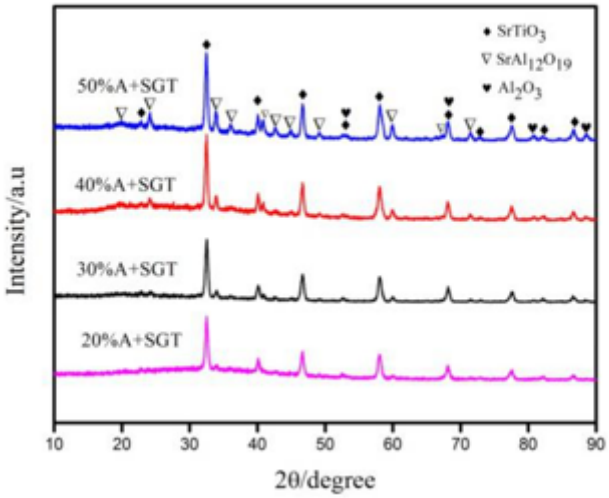

Figure 1

XRD patterns of xAl2O3-(1-x)Sr0.85Gd0.15TiO3 ceramics at various x values.

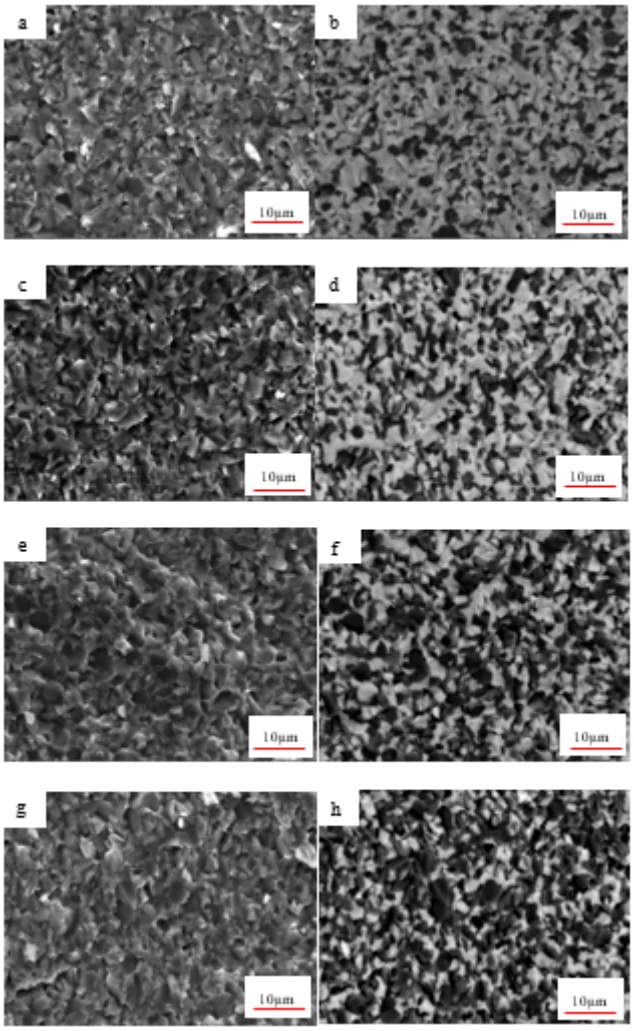

Figure 2

SEM secondary electron (SE) photographs (a, c, e, g) and backscattered electron (BSE) photographs (b, d, f, h) of the fractured cross-sections of xAl2O3-(1-x)Sr0.85Gd0.15TiO3 ceramic samples (a and b: x=0.2, c and d: x=0.3, e and f: x=0.4, g and h: x=0.5).

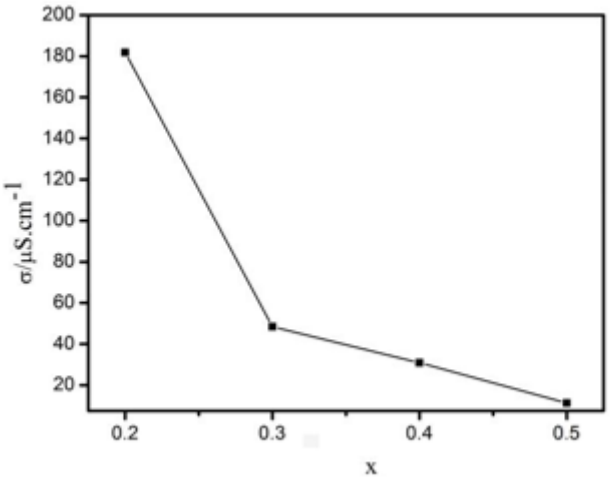

Figure 3

Electrical conductivity of xAl2O3-(1-x)Sr0.85Gd0.15TiO3 ceramic samples.

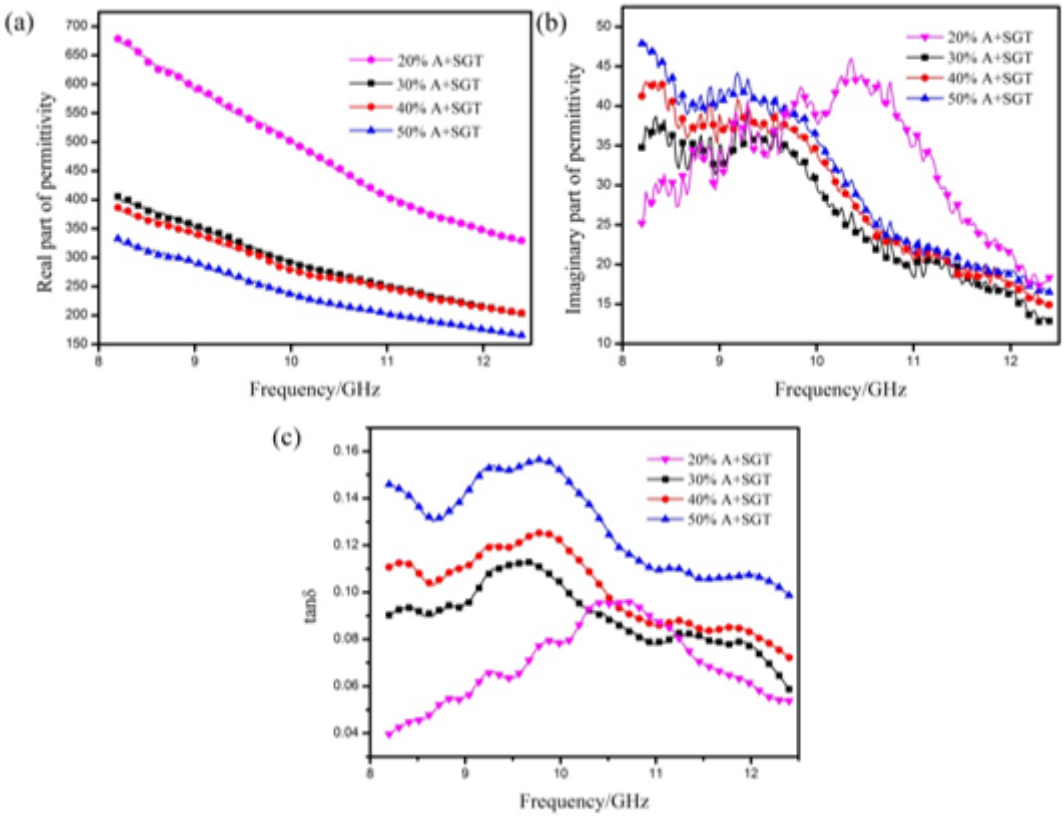

Figure 4

Frequency-dependent (a) real part, (b) imaginary part, and (c) loss tangent of the permittivity of xAl2O3-(1-x)Sr0.85Gd0.15TiO3 ceramics.

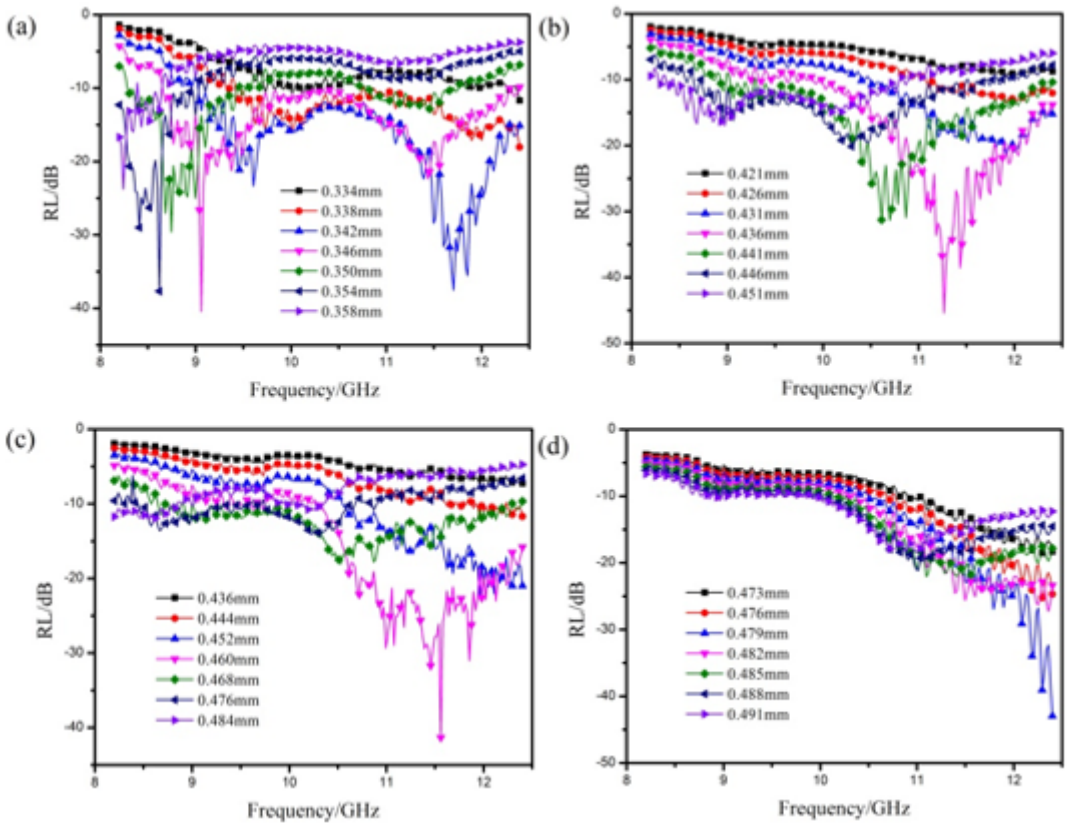

Figure 5

Reflection loss of xAl2O3-(1-x)Sr0.85Gd0.15TiO3 ceramics with different thicknesses: (a) x=0.2, (b) x=0.3, (c) x=0.4, and (d) x=0.5.

Supplementary Files

This is a list of supplementary files associated with this preprint. Click to download.

- ResultandDiscussionwithEquations.docx